(This is a sample cover image for this issue. The actual cover is not yet available at this time.)

Earth and Planetary Science Letters 353–354 (2012) 72–81

Contents lists available at SciVerse ScienceDirect

Earth and Planetary Science Letters

journal homepage: www.elsevier.com/locate/epsl

An empirical scaling of shear-induced outgassing during magma ascent: Intermittent magma ascent causes effective outgassing

Atsuko Namiki *

Department of Earth and Planetary Science, University of Tokyo, 7-3-1, Hongo, Bunkyo, Tokyo 113-0033, Japan

ARTICLE INFO

Article history:
Accepted 8 August 2012
Editor: T. Elliot

Keywords:
outgassing
shear localization
bubbly magma
Capillary number

ABSTRACT

Outgassing, which changes the distribution of volcanic gases in magmas, is one of the most important processes to determine the eruption styles. Shear deformation of ascending bubbly magmas at the vicinity of the volcanic conduit wall has been considered as an efficient mechanism of outgassing. On the other hand, seismological observations of volcanic eruptions reveal the gas bursting associated with long-period (LP) earthquakes and tremors, suggesting the existence of a large void space in the conduit. However both, the quantitative features of shear-induced outgassing and a mechanism to make a large void space, have still remain unknown. Here I perform a series of model experiments in which shear localization of syrup foam causes outgassing by making large bubbles or a crack-like void space, likely a gas bursting source. There is a critical strain, γ, above which outgassing occurs depending on the Capillary number, Ca, $\gamma > 1$ for $Ca < 1$ and $\gamma > Ca^{-1}$ for $Ca \geq 1$. The width of the region in which outgassing occurs is described as a function of $\gamma^{0.48}Ca^{0.24}$. Outgassing occurs efficiently at the very beginning of the deformation, suggesting that intermittent magma ascent causes effective outgassing such that the eruption style becomes effusive. This hypothesis is consistent with the fact that cyclic activity has been observed during effusive dome eruptions.

1. Introduction

Distributions of volcanic gases in magmas cause variety of eruption styles (Eichelberger et al., 1986; Wallace, 2001; Ripepe et al., 2005; Parfitt and Wilson, 2008; Shinohara, 2008; Houghton et al., 2010). Since magmas in themselves are incompressible, only the magmas containing compressible bubbles subject to decompression can erupt explosively (Namiki and Manga, 2005). Magmas without bubbles erupt effusively or sometimes does not reach to the Earth's surface (Shinohara, 2008).

A permeable flow through the interconnected bubbles may change gas distributions in magmas (Eichelberger et al., 1986; Klug and Cashman, 1996; Melnik et al., 2005; Kozono and Koyaguchi, 2009), but interconnected bubbles appear only for the volume fraction of bubbles > 0.7 (Namiki and Manga, 2008; Takeuchi et al., 2009). In addition, when magma viscosity is low, the interconnected bubbles may deform to become impermeable because of the surface tension and gravitational forces.

An alternative mechanism of outgassing is shear-induced magma fragmentation (Goto, 1999; Gonnermann and Manga, 2003; Tuffen et al., 2008). Shear-induced fragmentation may cause stick-slip at the conduit wall and makes the magma ascent intermittent (Denlinger and Hoblitt, 1999; Voight et al., 1999; Iverson et al., 2006). Shear-induced fragmentation occurs when the time scale of the deformation is sufficiently faster than the relaxation time scale of the magma depending on the viscosity (e.g., Webb and Dingwell, 1990). Viscosity of magma increases at shallower depth by exsolution of volcanic gases. Shear-induced fragmentation must be an effective process at a shallow part of the conduit. The gas originated from the deep conduit may outgas through this fracture plane. However, the manner in which the gas trapped inside each tiny bubble gathers into the fracture plane is not obvious.

Shear deformation itself, even without fragmentation, around the conduit wall has an important role on the outgassing. Shear deformation makes the bubbles in magma interconnected (Okumura et al., 2008), resulting that the gas permeability increases (Okumura et al., 2009) and outgassing occurs by compaction (Okumura et al., 2010). An large strain effectively increases the permeability (Okumura et al., 2009; Caricchi et al., 2011).

The shear deformation of bubbly fluid sometimes localizes (Schall and van Hecke, 2010). Debregeas et al. (2001) show shear localization of 2D foam at the vicinity of the moving wall in which flow rate decays exponentially. Wang et al. (2006) show that the occurrence of shear localization depends on the boundary condition. Janiaud et al. (2006) introduce an idea of the drag force arisen from boundary conditions and analytically makes a regime diagram of the shear localization. Katgert et al. (2009) shear 2D foam layer and makes a model to explain its velocity profile.

* Tel.: +81 3 5841 4670; fax: + 81 3 5841 8791.
E-mail address: namiki@eps.s.u-tokyo.ac.jp

0012-821X/$ - see front matter © 2012 Elsevier B.V. All rights reserved.
http://dx.doi.org/10.1016/j.epsl.2012.08.007

However, a quantitative formulation to estimate the outgassed volume by localized shear deformation is still lacking.

Another possible morphology of volcanic gasses in the conduit is gas-rich void spaces. An explosive gas emission associated with long-period (LP) earthquakes (Fischer et al., 1994; Johnson et al., 2008; Chouet et al., 2010; Kazahaya et al., 2011) suggests that the large amount of volcanic gas is once accumulated in a large void space to flow into a crack quickly and to excite LP earthquakes. The void space may have an annular shape and cause tremor (Jellinek and Bercovici, 2011). On the other hand, decompression associated with magma ascent usually makes numerous tiny bubbles (e.g., Hurwitz and Navon, 1994; Mourtada-Bonnefoi and Laporte, 2004). The explanation of the mechanism to make a large void space is also still lacking.

Here I impose shear deformation on syrup foam in order to quantitatively estimate the effect of the shear deformation on outgassing. Experiments provide an empirical scaling to evaluate the outgassed volume from ascending magmas.

2. Experimental methods

The experiment simulates the shear deformation of bubbly magma ascending in a volcanic conduit (Fig. 1). By using syrup foam as an analogue of bubbly magma, experiments are conducted under a room temperature and atmospheric pressure.

The experimental tank has inner dimensions of 380 mm height, 125 mm width and 49 mm depth and is equipped with a moving (timing) belt as a parallel band device (Taylor, 1934; Rust and Manga, 2002a). The moving belt shears the syrup foam, which has a 600 mm perimeter, 30 mm width, and 3.4 and 1.4 mm teeth inside and outside, respectively. A pulley activating the moving belt is mounted to a stepping motor (NSK Megatorque motors) with a variable rotation rate that determines the shear velocity (1.8×10^{-4}–$0.44\ \mathrm{m\ s^{-1}}$) and a rotation angle that determines displacement h (1.8×10^{-3}– 7.7 m). The distance between the tank wall and the moving belt is l=29 mm. The strain ($0.06\le\gamma\le300$) is calculated by the ratio of displacement and the distance between the belt and the tank wall $\gamma=h/l$. In most experiments, the space surrounded by the moving belt (gray region in Fig. 1) is filled with foamed polystyrene so that shear-induced outgassing does not occur in this space.

The method to calculate the shear rate ($0.006\le\dot{\gamma}\le15$) depends on the duration to activate the moving belt. The rotation rate of the motor is first accelerated, maintained at a constant velocity, v_c, and then decelerated. The time required for each acceleration and deceleration is 0.1 s. In experiments in which the activating duration is longer than 0.2 s, the shear rate is calculated by the ratio of the constant velocity to the distance between the tank wall and the moving belt, $\dot{\gamma}=v_c/l$. The time duration for the deformation Δt is calculated by the displacement and constant velocity $\Delta t=h/v_c$. In experiments in which the time for activation is shorter than 0.2 s, there are no regimes with a constant velocity. The mean velocity v_m during the deformation is used to calculate the shear rate, $\dot{\gamma}=v_m/l$, and the time duration for the deformation $\Delta t=h/v_m$.

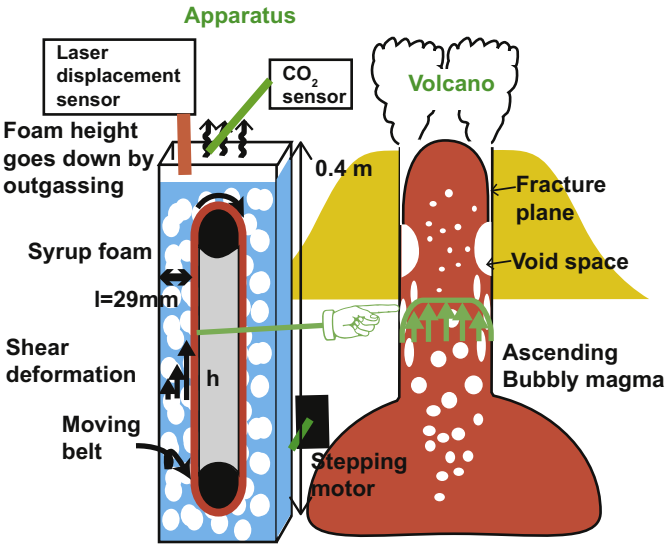

Fig. 1. Schematic diagram of the experimental apparatus and applicable place in a volcanic conduit.

For a magma analogue, I use syrup and introduce bubbles through a chemical reaction of baking soda and citric acid, which generates CO_2 gas. This is the same technique used in Namiki and Manga (2008). The syrup is a Newtonian fluid and surfactant free, and is appropriate for a magma analogue. The viscosity of the syrup is varied by changing the water content in the range of $50\le\eta\le500$ Pa s. This range overlaps with basaltic magma and some part of the pre-eruptive andesitic magma (Takeuchi, 2011). The surface tension of syrup is estimated as same as that for water $\sigma=0.07\ \mathrm{N\ m^{-1}}$, and is the same orders of magnitude as those of real magma (e.g., Mangan and Sisson, 2005). The minimum bubble diameter which corresponds to the size of the most abundant bubbles is in the range of $0.06<D<0.9$ mm with an average of 0.3 mm. This is the same orders of magnitude as those in real magmas (e.g., Klug and Cashman, 1994). Bubble size is measured by using macro photography. The volume fraction of bubbles is controlled in two ways, by changing the amount of the foaming agents, and by waiting until the foam reaches to the volume fraction of bubbles at which I desire to run the shear deformation. The volume fraction of bubbles in the foam ($0.16<\phi<0.81$) is calculated from the weight of the syrup and the foam volume.

The outgassed volume is measured by the decreases in the foam volume. Decreases in the foam volume indicate that the gas which has been trapped in the bubbles escapes to the atmosphere. This is because the volume of the syrup and CO_2 gas does not change significantly within the variation of room temperatures and atmospheric pressures during a short time span to measure the outgassed volume. The effects of the dissolution and exsolution of CO_2 gas caused by the fluctuation of the room temperature and atmospheric pressure in a short time scale are also limited. The measured outgassed volume can be a minimum estimate, because a chemical reaction may supply newly generated gas to increase the foam volume. The foam volume is calculated from its side view assuming that the height of the foam is uniform in depth. Since outgassing occurs by the coalescence of bubbles without nucleation and growth of bubbles, the outgassing observed in this experiment is applicable to a real magma system irrespective of gas species.

For the visual observation, a digital camera with resolutions of 2560×1920 or 3264×2448 pixels and a digital video camera with resolutions of 1920×1080 at 30 frames/s are used. The syrup is quite viscous, thus, when the foam volume decreases, it adheres to the tank wall, making it difficult to determine the actual volume change. The tank is illuminated from behind to make it possible to observe the height of the foam. In some experiments, the syrup on the wall is scraped off after the foam volume decreases, whose weight is less than 2 wt% of the entire weight of the syrup. The effect of the adhered syrup to estimate the volume fraction of bubbles in the foam is limited.

A laser displacement sensor (Keyence LB-10/60) measures a time series of foam height at a restricted point. The measurable span is 80 mm. A CO_2 sensor (VAISALA GM70) measures a time series of CO_2 gas concentration during the outgassing. On the CO_2 measurement, only the variations in the measured value are discussed rather than the absolute values. This is because,

the absolute value of the measured CO_2 concentration depends not only on the outgassed volume but also on the distance between the surface and the sensor. The distance between the sensor and the surface is time-dependent. The response time of the sensor is longer than 30 s.

The experimental procedure is as follows. First, I stir the syrup and chemicals in a beaker, and then pour it into the experimental tank. After the foam expands sufficiently, shear deformation is imposed on the foam. When the decreasing foam volume stops, the shear deformation is imposed again on the same foam but with a different initial volume fraction of bubbles. Each shear deformation is 'an experiment.' When most gas in the foam outgases, the series of the experiment is terminated. I perform 11 series of 81 experiments.

3. Results

3.1. Visual observations

Fig. 2a and Animation 1 are an overview of a series of experiments. At first, the foam expands because of the chemical reaction. Some large bubbles appear in the foam and ascend to the surface. When the bubbles burst, the surface deflates, and the measured CO_2 concentration above the foam increases. Even without shear deformation, some amount of gas escapes from the foam by ascending as large bubbles.

Supplementary Animation 1 associated with this article can be found in the online version of http://dx.doi.org/10.1016/j.epsl.2012.08.007.

When the foam is deformed, extensive outgassing occurs. At 16 h, shear deformation is imposed on the foam by the moving belt, and a void space appears beneath the top of the foam. This is because the shear deformation makes large bubbles efficiently, as shown by an orange circle, and gas ascends as large bubbles. The surface of the foam, however, locally has large viscosity by the evaporation of water and makes an undeformable crust. Beneath the crust, gas accumulates. This may be a process to make a gas layer beneath an impermeable lava dome. At the timing denoted by the light blue line, the crust is removed manually, and the measured CO_2 concentration rises, indicating that the gas is CO_2 and originated within the bubbles.

Fig. 2b and Animation 2 provides details of experiment 3 in Fig. 2a. Again, a large bubble appears, as shown by an orange circle at 19.2 h. The large bubble reaches to the surface, and then the measured CO_2 concentration increases as shown by the yellow curve in Fig. 2a and Animation 2. The observed asymmetric shape of the yellow curve which is sharp rises and slow drops (Fig. 2a) is

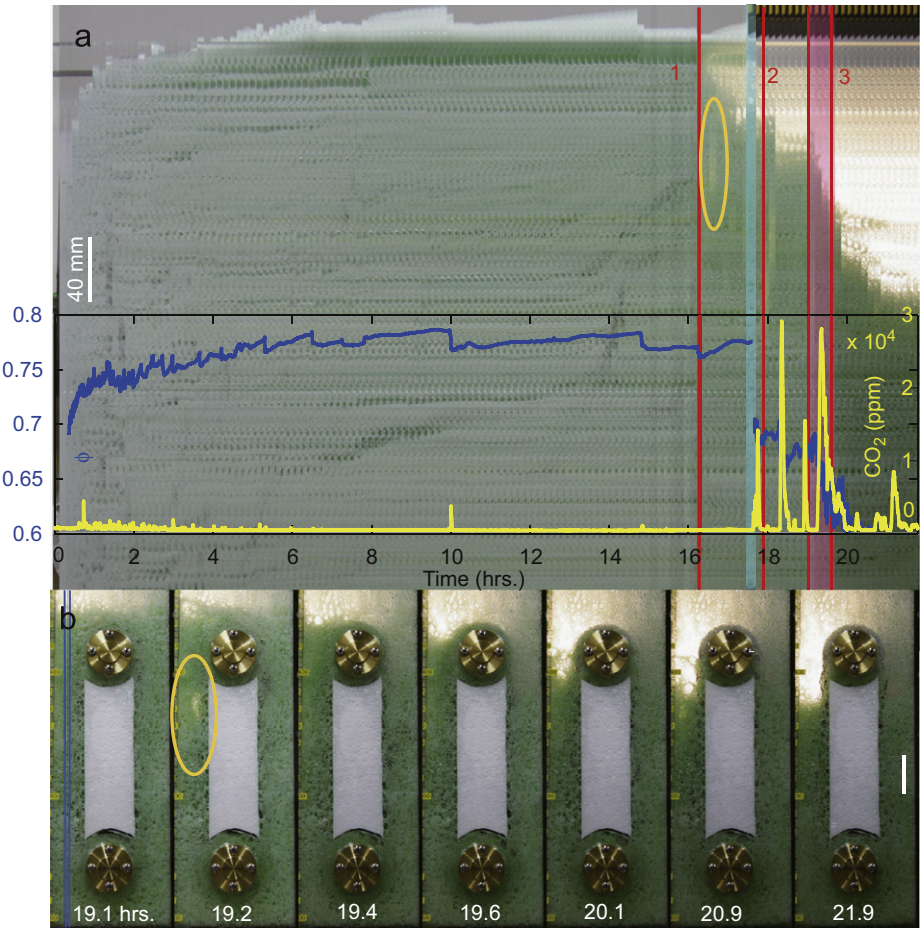

Fig. 2. (a) Time evolution of the foam height by visual observations in the range indicated by blue lines in (b). Time increases towards the right side in 10-min intervals, and the total time span is 22 h. Red lines indicate the timing of three experiments in which shear deformation is imposed. The imposed strain γ and shear rate $\dot{\gamma}$ for experiments 1, 2 and 3 are $\gamma = 6$ & $\dot{\gamma} = 0.03$, $\gamma = 1$ & $\dot{\gamma} = 0.03$, and $\gamma = 12$ & $\dot{\gamma} = 0.006$, respectively. Experiment 3 lasted 33 min. The orange circle indicates a large bubble generated by shear deformation. The blue curve in the graph indicates the calculated volume fraction of the bubbles. The volume of the foam is calculated by using the height measured by the laser displacement sensor. The yellow curve indicates the CO_2 concentration above the foam. At the timing indicated by the light blue line, the crust of syrup is removed manually and both the displacement and CO_2 sensors are moved 60 mm downwards. (b) Side view of the foam during and after experiment 3. The numbers indicate time (h) and correspond to the graph in (a). White bars in (a,b) indicate 40 mm. (For interpretation of the references to color in this figure caption, the reader is referred to the web version of this article.)

similar to the time series of volcanic gas measurements during explosive gas emissions and Strombolian eruptions (Edmonds et al., 2003; Burton et al., 2007).

Supplementary Animation 2 associated with this article can be found in the online version of http://dx.doi.org/10.1016/j.epsl.2012.08.007.

Fig. 3a and Animation 3 show the foam during and after the fast deformation, $\gamma = 1$ and $\dot{\gamma} = 3$. Bubbles only near the moving belt elongate as indicated by a pink circle, suggesting that shear localization occurs. Shear localization has also been observed in experiments with real magmas (Okumura et al., 2010). The surface of the foam goes down particularly in the region close to the moving belt as denoted by the pink arrow. This is because the interconnected bubbles which appear during the coalescence are immediately separates into a large void and bubble-free liquid by surface tension and gravitational forces. The large void is also recognized in the top view as indicated by the pink allow in Fig. 3b and Animation 3. The gravitational flow fulfills the void space. Finally, the volume fraction of bubbles locally decreases in the vicinity of the moving belt, which is evident by the color of the foam at 180 s; foam with more bubbles is whitish, and that with less bubbles is greenish. This result indicates that localization of shear deformation and outgassing occurs in the vicinity of the moving belt.

Supplementary Animation 3 associated with this article can be found in the online version of http://dx.doi.org/10.1016/j.epsl.2012.08.007.

3.2. A regime diagram of outgassing

Fig. 4 summaries the experimental results. The vertical axis is the strain γ. The horizontal axis is the Capillary number, defined as

$$\mathrm{Ca} = \frac{\eta \dot{\gamma} D}{\sigma}, \tag{1}$$

where D is the minimum and most abundant bubble diameter observed in each experiment, and η is viscosity of the syrup for each experiment. When the strain exceeds 1, the outgassing arises in most of experiments irrespective of Ca. The experiments in the regime $\gamma > 1$, but outgassing is not observed, are conducted during the syrup foam is expanding. Gas generation can compensate for outgassing. I thus define $\gamma > 1$ as the outgassing threshold for $\mathrm{Ca} < 1$. For $\mathrm{Ca} \geq 1$, experiments with $\gamma < \mathrm{Ca}^{-1}$ show outgassing.

3.3. The width of the outgassing region

Fig. 5a,b shows that the outgassed volume depends both on the strain, γ, and the volume fraction of bubbles, ϕ. Comparing the

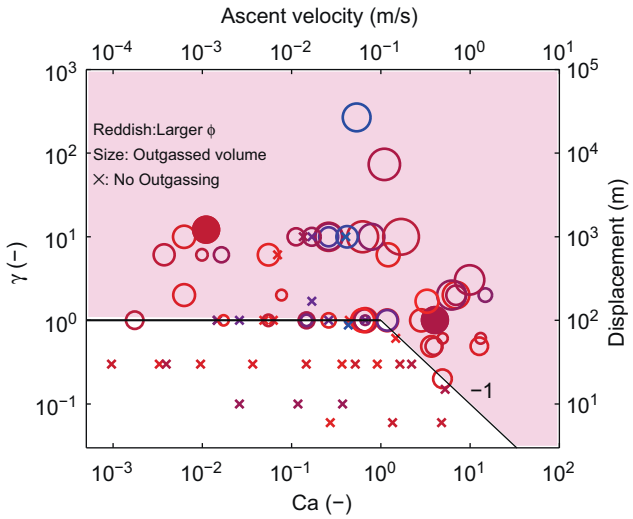

Fig. 4. Regime diagram of outgassing from a sheared foam as a function of the strain and the Capillary number defined in Eq. (1). The circles indicate the occurrence of outgassing, and the crosses indicate its absence. The circle sizes indicate the outgassed volume in a logarithmic scale normalized by the gas volume initially trapped in the foam. Reddish and bluish symbols indicate a larger and lower volume fraction of bubbles in the foam, respectively. The solid symbols indicate the experiments shown in Figs. 2b and 3. The top horizontal axis indicates the corresponding ascent velocity of magma for the conduit radius $l = 100$ m, the viscosity of magma is 10^5 Pa s, the surface tension is 0.1 N m^{-1}, and the bubble diameter is 10^{-3} m. The vertical axis on the right-hand side indicates the ascent distance of the magma in an uplift event, γl, when the conduit radius is $l = 100$ m. (For interpretation of the references to color in this figure caption, the reader is referred to the web version of this article.)

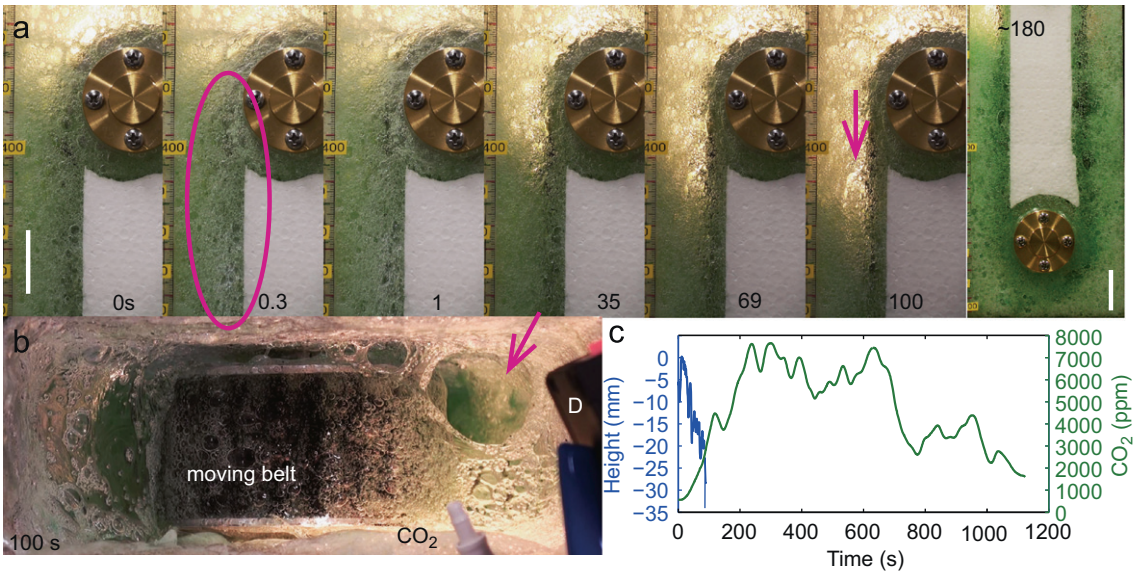

Fig. 3. (a) Side views of the foam during and after a fast shear deformation, $\gamma = 1$ and $\dot{\gamma} = 3$. The numbers indicate the time (s) elapsed after the deformation initiates. The pink circle indicates macroscopic shear localization. The pink arrow indicates a localized decrease in the foam height. White bars indicate 40 mm. (b) A top view of the sheared foam shown in (a) at 100 s. The pink arrow indicates a localized decrease of the foam height as shown in (a). The depth (vertical width in the picture) is 49 mm. (c) A time series of measured height of the foam (blue curve) and CO_2 concentration (green curve). The loci of the laser displacement sensor (D) and the inlet of the CO_2 sensor is shown in (b). At the beginning of this experiment, visually transparent large bubbles accumulate at the top of the foam. It is not obvious which part of the foam the laser displacement sensor measures. (For interpretation of the references to color in this figure caption, the reader is referred to the web version of this article.)

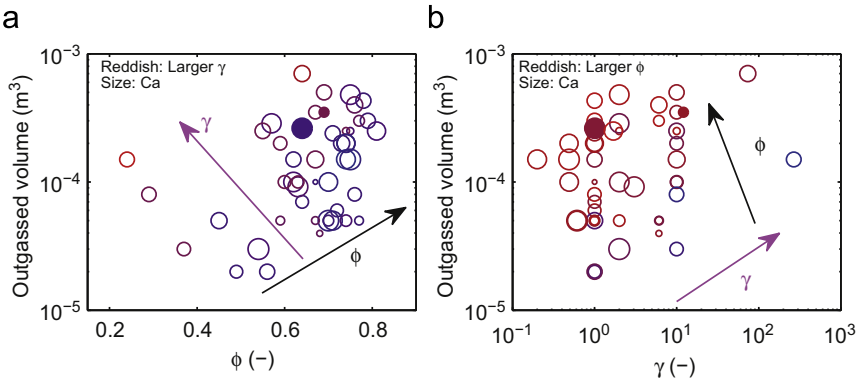

Fig. 5. (a,b) Measured outgassed volume depending on the volume fraction of bubbles, ϕ (a), and imposed strain, γ (b). The color of the symbols indicates the imposed strain or volume fraction of bubbles; reddish shows a larger value. The larger symbols indicate a higher Capillary number. The solid symbols indicate the experiments shown in Figs. 2b and 3. (For interpretation of the references to color in this figure caption, the reader is referred to the web version of this article.)

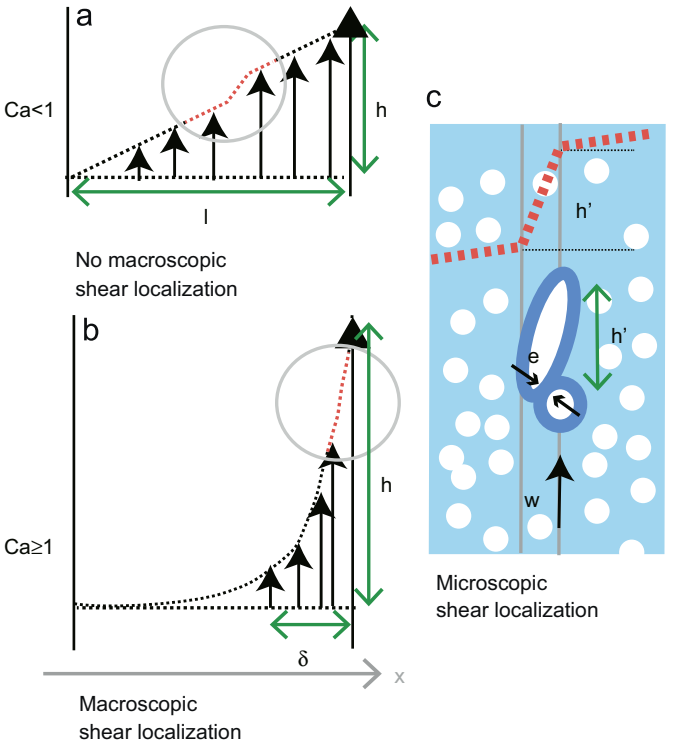

Fig. 6. (a) A schematical profile of displacement between the tank wall and the moving belt for Ca < 1, in which macroscopic shear localization does not appear but the microscopic (bubble size) shear localization occurs. (b) Same as (a) but for Ca ≥ 1, and macroscopic shear localization occurs. (c) A magnified view inside circles denoted in (a) and (b) indicating microscopic shear localization. Blue circles indicate bubbles under shear deformation. (For interpretation of the references to color in this figure caption, the reader is referred to the web version of this article.)

experiments with similar strains and the Capillary numbers, the outgassed volume increases as the volume fraction of bubbles increases, as denoted by black arrows. Similarly, the outgassed volume increases for a larger strain as shown by pink arrows.

From these facts and visual observations, I infer that there is a width W in which the deformation of the foam is extremely localized. Outgassing occurs exclusively within the region W as shown in Fig. 6. I refer this as an outgassing region. Although, inside the foam is opaque and is difficult to visually observe the details of the outgassing region, I infer that the elongated large bubbles appeared during the shear deformation as denoted by orange circles in Fig. 2 are manifestations of the outgassing region.

Following this hypothesis, the measured volume of the outgassing for each experiment becomes $V_o \sim \phi W L_b d$, where L_b is the length of the moving belt soaked in the foam measured by the visual observation and d is the horizontal depth of the experimental tank. Here V_o, ϕ, L_b, and d are measured values so that I obtain W.

Normalizing W by the minimum bubble diameter $W^* = W/D$, the non-dimensional width of the outgassing region becomes

$$W^* \sim \frac{V_o}{\phi L_b d D}. \tag{2}$$

In Fig. 7a, the non-dimensional width of the outgassing region W^* is plotted as a function of Ca, for each experiment, where the larger reddish and smaller bluish symbols indicate larger and smaller strain γ, respectively. Fig. 7a shows that the width of the outgassed region W^* weakly depends on the Capillary number, comparing the experiments with a same strain. I calculate slops for the experiments with strains around one $0.7 < \gamma < 2$ and around ten, $6 < \gamma < 20$, and then obtain similar values 0.21 and 0.27, respectively. I interpret this result as meaning that the slopes for each group with a same strain are similar, but the y-intercepts are different. The y-intercept increases as the imposed strain increases. Using the averaged value 0.24, the dependence of W^* on the Capillary number is written as

$$W^* \propto A(\gamma)\mathrm{Ca}^{0.24}. \tag{3}$$

Fig. 7b shows that the calculated prefactor $A(\gamma)$ for each experiment depends on strain γ with a slope of 0.48. Using these two empirical scalings, I obtain

$$W^* \sim 25\gamma^{0.48}\mathrm{Ca}^{0.24}, \tag{4}$$

where 25 is a constant empirically determined (Fig. 7b). Fig. 7c shows that the measured and calculate outgassed volume from Eq. (4) have positive correlation.

This result suggests that, during an experiment, the thickness of the outgassing region increases as the strain γ increases, but the thickening rate decelerates. Thickening rate should be important when applying these results to a real outgassing from ascending magma. Here direct measurement of temporal variation of W^* is quite difficult. This is because the foam is opaque. In addition, the descending rate of the foam height is regulated by the compaction than the thickening rate of W^*; i.e., the descending rate of the foam height measured by the laser displacement sensor represents the compaction velocity. I thus calculate W^* from integrated outgassed volume V_o.

Eq. (4) indicates that the thickness of the outgassing region, which determines the outgassed volume, depends on both the strain and the Capillary number, and is more sensitive to the strain γ. This result is consistent with that observed in the real magma in which large strains $\gamma > 8$ enhance outgassing (Okumura et al., 2009; Caricchi et al., 2011).

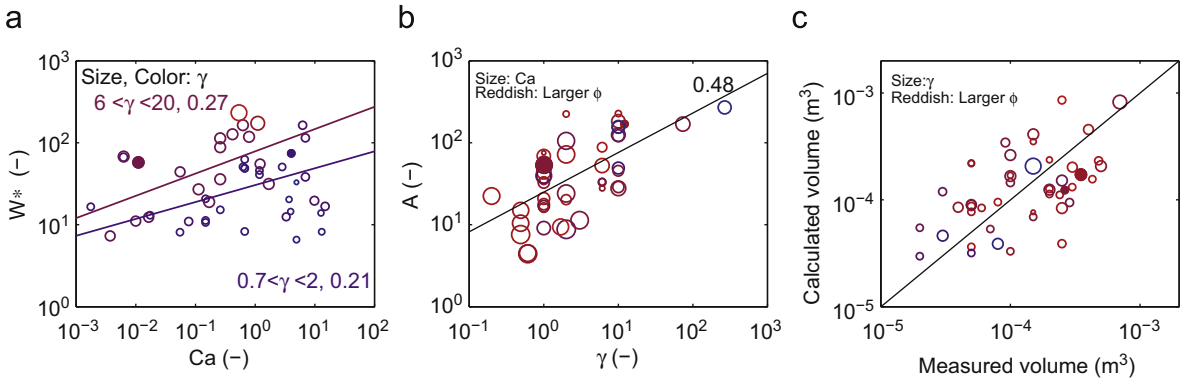

Fig. 7. (a) The width of the outgassing region which is defined by Eq. (2) as a function of the Capillary number. Large reddish and small bluish symbols indicate the larger and smaller imposed strain, γ, respectively. The calculated slopes for the experiments, $0.7<\gamma<2$ and $6<\gamma<20$ are 0.21 and 0.27, respectively. (b) Prefactor $A(\gamma)$ in Eq. (3) calculated for each experiment by $W^*/\mathrm{Ca}^{0.24}$. The size of the circle indicates the Capillary number, and the color indicates volume fraction of bubbles. (c) Comparison of the measured and calculated outgassed volume from Eq. (4). The size of the circle indicates the imposed strain, and the color indicates volume fraction of bubbles. In (a–c), the solid symbols indicate the experiments shown in Figs. 2b and 3. (For interpretation of the references to color in this figure caption, the reader is referred to the web version of this article.)

4. Discussion

These experiments show that when strain is large enough, outgassing occurs. The required strain for outgassing depends on the Capillary number (Fig. 4). This may be caused by the macroscopic shear localization (Fig. 6a,b). The measured outgassed volume suggests the existence of the microscopic shear localization within a width of W to cause outgassing (Figs. 6c and 7). I here consider the possible model of the macroscopic and microscopic shear localization from above empirical scalings.

4.1. The critical strain for outgassing

Fig. 4 shows that the threshold for outgassing is $\gamma>1$ for $\mathrm{Ca}<1$ and $\gamma>\mathrm{Ca}^{-1}$ for $\mathrm{Ca}\geq 1$. From this result, I infer that outgassing occurs when the effective strain exceeds unity, $\gamma_e>1$. The threshold, $\gamma_e>1$, suggests that some bubbles have to slide past each other when the bubbles are closely packed. When bubbles pass each other, they may coalesce and finally cause outgassing. In this paper, I define strain as a normalized displacement by the distance between the moving belt and the tank wall $\gamma=h/l$ (Fig. 6a). When the macroscopic displacement is localized in a width δ (Fig. 6b), $\gamma=h/l$ becomes a nominal strain. The effective strain is written as $\gamma_e=l\gamma/\delta$. The threshold for the outgassing is thus written as $\gamma>\delta/l$. The observed critical strain in Fig. 4 suggests that the width of the locally deformed region in a macroscopic view is scaled as

$$\delta\propto l\mathrm{Ca}^{-1}, \tag{5}$$

for $\mathrm{Ca}\geq 1$.

The idea that the width of the macroscopic localization depends on the Capillary number is consistent with a model for 2D disordered foam (Katgert et al., 2009). The essence of their model is that the velocity profile is determined by the balance of two forces act on a bubble. One is drag force gradient which may be a wall effect and is considered as a function of the local Capillary number Ca_l, $l^{-1}\mathrm{Ca}_l^{\zeta}$ (e.g., Bretherton, 1961; Denkov et al., 2005). The other is the gradient of the shear stress τ. Foam is considered as Herschel–Bulkley fluid (Herschel and Bulkley, 1926; Princen and Kiss , 1989) whose constitutive equation is

$$\tau=\tau_Y+f_{bb}\mathrm{Ca}_l^{\beta}, \tag{6}$$

where τ_Y is the yield stress and f_{bb} is a constant. The force balance is thus written as

$$\frac{d\tau}{dx}\propto \mathrm{Ca}_l^{\beta-1}\frac{d\mathrm{Ca}_l}{dx}\propto -l^{-1}\mathrm{Ca}_l^{\zeta}. \tag{7}$$

Using the boundary condition $\mathrm{Ca}_l\sim\mathrm{Ca}$ at $x=0$, the integration of this equation becomes $x\propto l\,(\mathrm{Ca}^{\beta-\zeta}-\mathrm{Ca}_l^{\beta-\zeta})$. The typical width of the locally deformed region in macroscopic view to be $\mathrm{Ca}_l\sim 0$ is scaled as $\delta\propto l\mathrm{Ca}^{\beta-\zeta}$.

In Katgert et al. (2009), $\beta=0.36$ and $\zeta=2/3$ is appropriate which results $\delta\propto l\,\mathrm{Ca}^{-0.3}$. The shape of the formula is the same but the absolute value of the exponent inferred from Fig. 4, $\delta\propto l\,\mathrm{Ca}^{-1}$, is different. The difference in the exponent may be arisen by following reasons. First, while my experiments are conducted with surfactant-free liquid, Katgert et al. (2009) perform their experiments with a surfactant solution. The existence of the surfactant affects the deformation of bubbles (e.g., Stone, 1994) which relates with β and ζ. Second, the range of the Capillary number in which experiments are conducted is different. The Capillary number in their experiments is lower than unity. On the other hand, my experiments are conducted in the range, $10^{-3}<\mathrm{Ca}<100$, including $\mathrm{Ca}=1$. In my experiments, macroscopic shear localization (Figs. 3, 6b) occurs for $\mathrm{Ca}\geq 1$ where the smallest bubble in the foam can deform (Eq. (1)). In a dilute bubbly fluid, the effective viscosity of the bubbly fluid is higher and lower than that of bubble-free liquid for $\mathrm{Ca}\ll 1$ and $\mathrm{Ca}\gg 1$, respectively (e.g., Rust and Manga, 2002b; Llewellin et al., 2002; Pal, 2003). Whether bubbles can deform determines the effect of the bubbles on the effective viscosity. I thus infer that the exponents β and ζ also depend on the range of the Capillary number.

4.2. A mechanism of shear-induced outgassing

Fig. 7a,b and Eq. (4) show an empirical scaling to evaluate the outgassed volume. I here consider the characteristics of the microscopic shear localization shown in Fig. 6c from the scaling of outgassed volume.

Fig. 4 and Eq. (4) suggest the following mechanism to cause shear-induced outgassing. Since bubble sizes in the syrup foam have variation and I define the Capillary number with minimum bubble size D in Eq. (1), there may exist a large bubble which satisfy individually $\mathrm{Ca}_i>1$ even for the regime $\mathrm{Ca}<1$. The bubble which satisfies $\mathrm{Ca}_i>1$ can deform as shown in Fig. 6c. Once a big bubble deforms significantly, shear stress required to continuously deform that region may decrease. Instability occurs and the

flow separates into bands of high and low shear rates (e.g., Schall and van Hecke, 2010). The deformation, thus, localizes at the lane of W where a large bubble exists (Fig. 6c).

I here consider the dependence of W on γ and Ca. In my experiments, the viscous force overwhelms the inertial force for each bubble, $\mathrm{Re}=\rho v_b D/\eta \ll 1$, where ρ is the density of syrup and v_b is the relative velocity of bubbles. Thus, the deformation of the foam surrounding a big bubble is considered as a creeping flow $\nabla p=\eta_e \nabla^2 v_b$, where η_e is the effective viscosity of the foam. When a big bubble is elongated by the shear deformation as shown in Fig. 6c, $W \ll h'$, lubrication approximation becomes appropriate (e.g., de Gennes et al., 2003). The vertical gradient of the Laplace pressure within a large bubble balances with the lateral gradient of the viscous stress,

$$\frac{\sigma}{h'D} \sim \frac{\eta_e v_b}{W^2}, \tag{8}$$

where I assume that the radius of the curvature at the tip of the elongated bubble is approximately the same as that of the smallest bubble. The local displacement should be related with the strain of the entire system, $h'/D \propto \gamma$. Since foam is considered as Herschel–Bulkley fluid (Eq. (6)), the effective viscosity of foam is written in the form of $\eta_e \sim \eta \mathrm{Ca}^{\beta-1}$. The Capillary number is also expressed by the relative velocity of bubbles $\mathrm{Ca} \sim \eta v_b/\sigma$. The width W is thus written as

$$W \sim \gamma^{1/2} \mathrm{Ca}^{\beta/2} D. \tag{9}$$

In Eq. (9), the dependence of W on γ has a power of 1/2, which is close to that experimentally obtained value 0.48 in Eq. (4). The dependence of W on Ca has a power of $\beta/2$. If the effective viscosity of the foam decreases as a shear rate increases, $\beta<1$, the dependence of W on Ca becomes less sensitive than that of γ. This result is also consistent with experimentally obtained Eq. (4).

The outgassed volume estimated from the model shown in Fig. 6c should depend on the abundance of large bubbles which is not formulated both in Eqs. (4) and (9). In Fig. 7c, the measured and calculated outgassed volumes from Eq. (4) do not correlate well. This may be because my model does not take into account the effect of the bubble size distribution.

In a narrow lane of the deformation, smaller bubbles cannot leave behind a large bubble. Since Eq. (8) suggests that even a minimum bubble can deform in this lane, bubbles deform and the surrounding film stretches continuously. When the film thickness e becomes thinner than a critical (Kobayashi et al., 2010), the film ruptures. Small bubbles thus coalesce into a large bubble. This idea is consistent with the explanation for the outgassing threshold. The threshold for the outgassing, an effective strain exceeds unity $\gamma_e>1$, suggests that some bubbles fail to slide past each other and coalesce into a large bubble.

Once all bubble films in this deformable lane rupture, bubbles become interconnected. The interconnected bubbles are unstable and separate into a large void and a bubble-free liquid. If the void connects to the atmosphere, outgassing occurs. If not, the void becomes a large bubble as denoted by the orange circles in Fig. 2.

5. Implications for a volcanic outgassing

Next, I apply the experimentally obtained scaling, Eq. (4), to the outgassing during a magma ascent in a volcanic conduit. In a magma ascent, the Reynolds number for the melt surrounding a bubble is considered as less than unity, $\mathrm{Re}=\rho v D/\eta \ll 1$, where v is the ascent velocity of the magma and ρ is the density of bubble-free melt. Since experiments are also conducted under $\mathrm{Re} \ll 1$, and Eq. (4) is written in a non-dimensional form, Eq. (4) is applicable to a real magma ascent unless viscosity of the magma is large enough to cause fragmentation.

Fig. 8a shows the estimated thickness of the outgassing region as a function of magma ascending distance which is considered as displacement, h. From Eq. (4) and $W^*=W/D$ the thickness of the outgassing region is written as

$$W=25\left(\frac{h}{l}\right)^{0.48}\left(\frac{\eta v D/l}{\sigma}\right)^{0.24} D. \tag{10}$$

I here assume that the viscosity of magma is $\eta=10^5$ Pa s, the surface tension is $\sigma=0.1$ N m^{-1}, ascent velocity of magma is $v=1$ m s^{-1}, and the bubble diameter is 10^{-3}m. These are the same as those in Fig. 4.

The solid lines show continuous magma ascent with a bubble diameter of 10^{-3} m. The different colors, red, blue, and green, indicate conduit radius $l=1$, 10, and 100 m, respectively. The circles indicate that the thickness of the outgassing region reaches the conduit center, suggesting that outgassing is accomplished. When the magma ascent is continuous, only the case with the narrowest conduit radius 1 m can accomplish outgassing (solid red line). Since the thickness of the outgassing region W depends on the conduit radius $l^{-0.72}$ as shown in Eq. (10), smaller l makes W increase. In addition, when the conduit radius l is narrow, the required W to accomplish outgassing becomes small. Thus, a narrow conduit causes effective outgassing.

The green line begins at a height of 10 m. This is because there is a minimum strain to cause outgassing (Fig. 4). When magmas ascend in a conduit with a radius of 100 m with a condition of $\mathrm{Ca} \sim 10$, outgassing begins when the strain exceeds 1/10 which corresponds to an ascending distance of 10 m.

The dashed blue line shows the case with the same conduit radius of solid blue line but with a smaller bubble diameter of 10^{-4} m. Since the width of the outgassing region W depends on $D^{1.24}$ in Eq. (10), smaller bubbles result in inefficient outgassing. The typical size of bubbles in ascending magmas is the order of a magnitude of 10^{-4} m. A bubble size of 10^{-3} m is slightly larger than a typical size (e.g., Klug and Cashman, 1994). I infer that the shear-induced outgassing is an effective mechanism for previously coarse graining bubbles by other mechanisms, such as bubble expansion and growth.

Magmas sometimes ascend intermittently as observed during dome growth (Denlinger and Hoblitt, 1999; Voight et al., 1999; Iverson et al., 2006). When magma ascent stops, deformed bubbles in magmas can relax. The gas within the interconnected bubbles may be able to outgas before magmas resume ascending. In such cases, the strain h/l should be calculated for each step. Eq. (10) is modified as

$$W=25\left(\frac{\Delta h}{l}\right)^{0.48}\left(\frac{\eta v D/l}{\sigma}\right)^{0.24} D\frac{h}{\Delta h}, \tag{11}$$

where Δh is the height of each uplift of the intermittent ascent.

The crosses and its overlapping in Fig. 8a show the thickness of the outgassing region for intermittent magma ascent with uplift events of 1 m each at a velocity of 1 m s^{-1}. When the conduit radius is 1 m (red) or 10 m (blue), intermittent magma ascent more effectively thickens the outgassing region than continuous one. When a magma with a bubble size of 10^{-3} m ascends continuously in a conduit with a radius of 10 m (blue solid line), only the region with a width of 2 m outgases for 10 km ascent. Magma chambers usually exist at shallower than 10 km. This result suggests that the magma reaches the surface of the Earth without complete outgassing. Intermittent magma ascent (blue crosses), however, the thickness of the outgassing region reaches the center of the conduit, and outgassing is accomplished (blue circle) for a 500 m ascent. This is because the thickness of the outgassing region depends on $\gamma^{0.48}$, indicating that the outgassing region more efficiently thickens at the very beginning of each ascent.

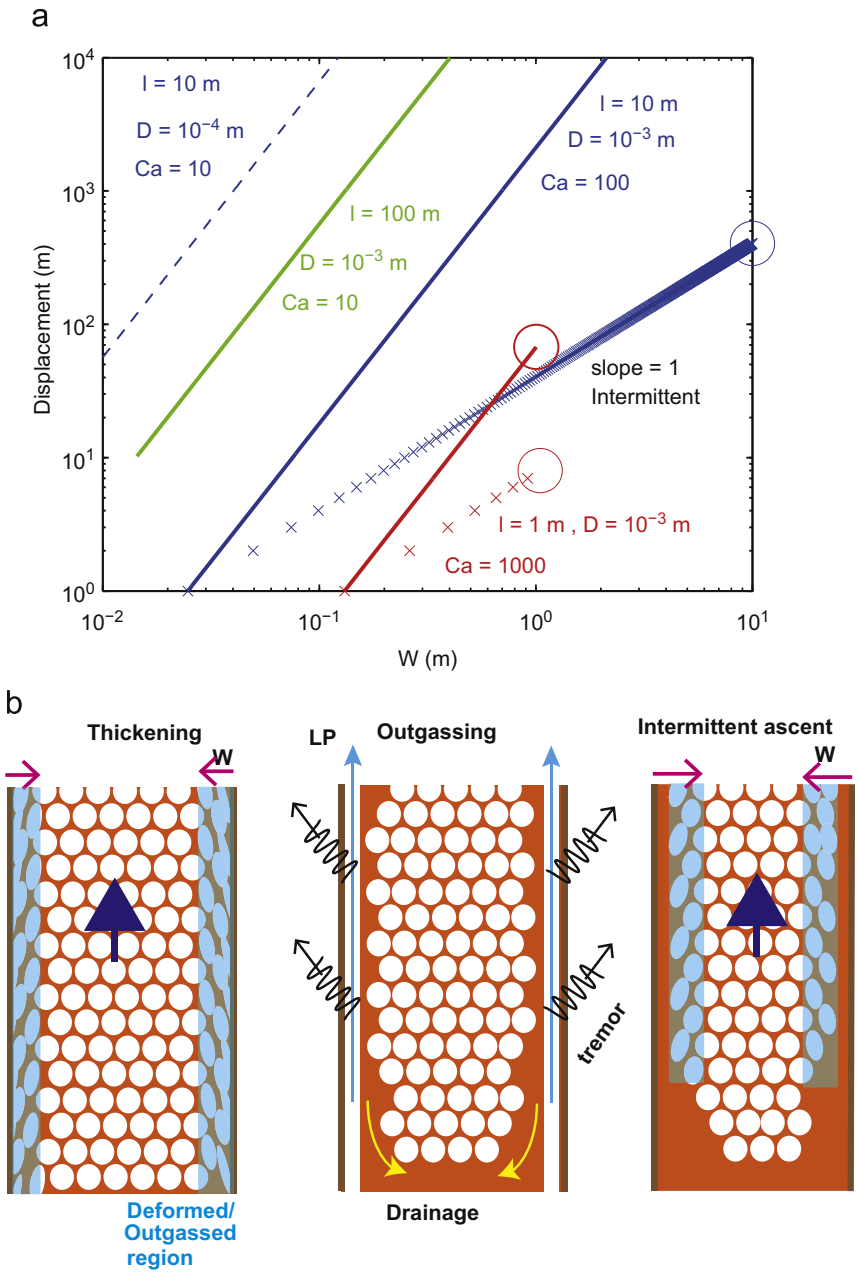

Fig. 8. (a) The estimated thickness of the outgassing region as a function of magma ascending distance (displacement). The solid and dashed lines show continuous magma ascent at a velocity of 1 m s^{-1} with a bubble diameter of 10^{-3} m and 10^{-4} m, respectively. The crosses and its overlapping show the thickness of the outgassing region for intermittent magma ascent with uplift events of 1 m each at a velocity of 1 m s^{-1}. The circles indicate that the thickness of the outgassing region reaches the conduit center, suggesting that outgassing is accomplished. The different colors, red, blue, and green, indicate conduit radius 1, 10, and 100 m, respectively. Other parameters are the same as those in Fig. 4. (b) Schematic diagram of outgassing. During a magma ascent, shear deformation of bubbles localizes around the conduit wall (left). The deformed bubbles become interconnected, and outgassing occurs. The interconnected bubbles are unstable and separate into a large void (an annulus or large bubbles) and bubble-free liquid (middle). The gas inside the annulus escapes to the atmosphere with exciting LP events or tremor, and then the conduit is refilled. Since only the bubble-rich region has buoyancy, the subsequent shear deformation is localized at the boundary between the bubble-rich and -poor regions (right). Repeating of this process causes intermittent outgassing. (For interpretation of the references to color in this figure caption, the reader is referred to the web version of this article.)

Even for an intermittent magma ascent, when each uplift event causes only a small strain, outgassing does not occur. For example, when the conduit radius is 100 m and each uplift event is 1 m at 1 m s^{-1}, outgassing does not occur (Fig. 4, top and right axes). The conduit radius of Mt. Unzen during the active dome eruption stage at the nucleation depth of microlites is approximately 10 m (Noguchi et al., 2008). Intermittent magma ascent could make outgassing efficiently.

I thus propose that outgassing occurs efficiently when magmas ascend intermittently in a narrow conduit associated with sufficiently large each uplift event. Fig. 8b shows an image of outgassing in a conduit during an intermittent magma ascent inferred from the experimental results. The outgassing region develops in the locally deformed region, which makes a gas annulus. If the annulus continues to the atmosphere, outgassing is accomplished immediately. If there exists an impermeable dome at the top of the conduit, the gas may accumulate beneath the dome (Fig. 1). The gas in the void space may erupt out through the fracture plane surrounding the dome at the next dome uplift event. Such a void space could become a source of an LP event. The timing of intermittent magma ascent is determined by the dome uplift event. If the void space is directly contact to the

country rock, the outgassing to the country rock is also enhanced (Jaupart and Allegre, 1991). Otherwise, each tiny bubble is surrounded by a melt film. Outgassing through the melt film to the country rock is inefficient. After the outgassing, bubble-free melt region is generated in a bubbly magma (Fig. 3a, 180 s). Bubble-free obsidian layers within a matrix of vesicular pumice may be generated in this manner (Manga et al., 1998). This hypothesis is consistent with the fact that cyclic activity has been observed during effusive dome eruptions (Denlinger and Hoblitt, 1999; Voight et al., 1999; Iverson et al., 2006).

If a magma ascends intermittently and each uplift event causes outgassing, the volcanic gas emission rate should show a variation in short time scales. This is consistent with what observed in Soufriere Hills Volcano (Edmonds et al., 2003). When magma ascends intermittently, the averaged flow rate is reduced. This may explain why the non-explosive eruption style is sometimes related with slow magma ascent. However, this is not necessarily so. Continuous magma ascent in a conduit with a large radius and intermittent magma ascent associated with a small each uplift event can cause explosive eruption. In the Inyo volcanic chain, a rhyolite magma has ascended slowly at the same rates as the dome-building phases and erupts explosively (Castro and Gardner, 2008).

The source geometries have been frequently related to the waveform of LP event (Chouet et al., 2010). This is because the resonant frequency usually depends on the size of a resonator (Kobayashi et al., 2010; Jellinek and Bercovici, 2011). If the void space (Fig. 1) or a gas annulus (Fig. 8b) causes an LP event or tremor, we may be able to estimate the shape of the gas container and annuls from the waveform. The shape of the annulus allows us to evaluate the outgassed volume and the gas volume remaining in the magma, which directly controls the subsequent eruption styles.

6. Conclusions

In order to understand the shear-induced outgassing from a bubbly magma, I conducted shear deformation experiments of syrup foam including CO_2 gas as a magma analogue. When the imposed shear strain is large enough, the height of the foam decreases indicating that outgassing occurs. During the outgassing, large bubbles and crack-like void spaces appear in the foam. Measured CO_2 concentration above the foam increases as an evidence that the gas is came from the inside bubbles. When there is an impermeable layer above the foam, the gas accumulates beneath that layer.

The critical strain for outgassing is $\gamma > 1$ for $\mathrm{Ca} < 1$ and $\gamma > \mathrm{Ca}^{-1}$ for $\mathrm{Ca} \geq 1$. For $\mathrm{Ca} \geq 1$, macroscopic shear localization of foam occurs such that outgassing occurs even for $\gamma < 1$. The width of the region in which outgassing occurs is described as a function of $\gamma^{0.48}\mathrm{Ca}^{0.24}$. The value of the exponent smaller than unity in $\gamma^{0.48}$ indicates that outgassing efficiently occurs at the very beginning of the shear deformation.

I apply the experimental results to a real magma ascent and conclude that intermittent magma ascent in a narrow conduit associated with sufficiently large each uplift event causes effective outgassing such that the eruption style becomes effusive. If there is an impermeable dome at the top of the conduit, the gas can accumulate beneath the dome. Such an accumulated gas may cause gas bursting associated with an LP event and tremors. If we can evaluate γ and Ca for each uplift event from LP earthquakes or tremor, we may be able to estimate the gas volume fraction remaining in the magma which controls the subsequent eruption styles.

Acknowledgments

I thank H. Shinohara and S. Takeuchi for discussion. This work was supported by KAKENHI 19740281, 21740326, 24681035 and Sasakawa Scientific Research Grant 19-231.

Appendix A. Supplementary material

Supplementary data associated with this article can be found in the online version of http://dx.doi.org/10.1016/j.epsl.2012.08.007.

References

Bretherton, F.P., 1961. The motion of long bubbles in tubes. J. Fluid Mech. 10, 166–188.
Burton, M., Allard, P., Mure, F., Spina, A.L., 2007. Magmatic gas composition reveals the source depth of slug-driven Strombolian explosive activity. Science 317, 227–230.
Caricchi, L., Pommier, A., Pistone, M., Castro, J., Burgisser, A., Perugini, D., 2011. Strain-induced magma degassing: insights from simple-shear experiments on bubble bearing melts. Bull. Volcanol. 73, 1245–1257.
Castro, J.M., Gardner, J.E., 2008. Did magma ascent rate control the explosive–effusive transition at the Inyo volcanic chain, California? Geology 36, 279–282.
Chouet, B.A., Dawson, P.B., James, M.R., Lane, S.J., 2010. Seismic source mechanism of degassing bursts at Kilauea Volcano, Hawaii: results from waveform inversion in the 10–50 s band. J. Geophys. Res. 115, B09311, http://dx.doi.org/10.1029/2009JB006661.
de Gennes, P.-G., Brochard-Wyart, F., Quere, D., 2003. Gouttes, bulles, perles et ondes. Yoshioka Shoten, Kyoto.
Debregeas, G., Tabuteau, H., di Meglio, J.-M., 2001. Deformation and flow of a two-dimensional foam under continuous shear. Phys. Rev. Lett. 87, 178305.
Denkov, N.D., Subramanian, V., Gurovich, D., Lips, A., 2005. Wall slip and viscous dissipation in sheared foams: effect of surface mobility. Colloids Surf. A 263, 129–145.
Denlinger, R.P., Hoblitt, R.P., 1999. Cyclic eruptive behavior of silicic volcanoes. Geology 27, 459–462.
Edmonds, M., Oppenheimer, C., Pyle, D.M., Herd, R.A., Thompson, G., 2003. SO_2 emissions from Soufriere Hills Volcano and their relationship to conduit permeability, hydrothermal interaction and degassing regime. J. Volcanol. Geotherm. Res. 124, 23–43.
Eichelberger, J.C., Carrigan, C.R., Westrich, H.R., Price, R.H., 1986. Non-explosive silicic volcanism. Nature 323, 598–602.
Fischer, T.P., Morrissey, M.M., Calvache, V.M.L., Gomez, M.D., Torres, C.R., Stix, J., Williams, S.N., 1994. Correlations between SO_2 flux and long-period seismicity at Galeras volcano. Nature 368, 135–137.
Gonnermann, H.M., Manga, M., 2003. Explosive volcanism may not be an inevitable consequence of magma fragmentation. Nature 426, 432–435.
Goto, A., 1999. A new model for volcanic earthquake at Unzen Volcano: melt rupture model. Geophys. Res. Lett. 26, 2541–2544.
Herschel, W.H., Bulkley, R., 1926. Konsistenzmessungen von gummi-benzollosungen. Kolloid-Zeitschrift 39, 291–300.
Houghton, B.F., Carey, R.J., Cashman, K.V., Wilson, C.J.N., Hobden, B.J., Hammer, J.E., 2010. Diverse patterns of ascent, degassing, and eruption of rhyolite magma during the 1.8 ka Taupo eruptionnn New Zealand: evidence from clast vesicularity. J. Volcanol. Geotherm. Res. 195, 31–47.
Hurwitz, S., Navon, O., 1994. Bubble nucleation in rhyolitic melts: experiments at high pressure, temperature, and water content. Earth Planet. Sci. Lett. 122, 267–280.
Iverson, R.M., Dzurisin, D., Gardner, C.A., Gerlach, T.M., LaHusen, R.G., Lisowski, M., Major, J.J., Malone, S.D., Messerich, J.A., Moran, S.C., Pallister, J.S., Qamar, A.I., Schilling, S.P., Vallance, J.W., 2006. Dynamics of seismogenic volcanic extrusion at Mount St Helens in 2004–05. Nature 444, 439–443.
Janiaud, E., Weaire, D., Hutzler, S., 2006. Two-dimensional foam rheology with viscous drag. Phys. Rev. Lett. 97, 038302.
Jaupart, C., Allegre, C.J., 1991. Gas content, eruption rate and instabilities of eruption regime in silicic volcanoes. Earth Planet. Sci. Lett. 102, 413–429.
Jellinek, A.M., Bercovici, D., 2011. Seismic tremors and magma wagging during explosive volcanism. Nature 470, 522–525.
Johnson, J.B., Lees, J.M., Gerst, A., Sahagian, D., Varley, N., 2008. Long-period earthquakes and co-eruptive dome inflation seen with particle image velocimetry. Nature 456, 377–381.
Katgert, G., Latka, A., Mobius, M.E., van Hecke, M., 2009. Flow in linearly sheared two-dimensional foams: from bubble to bulk scale. Phys. Rev. E 79, 066318.
Kazahaya, R., Mori, T., Takeo, M., Ohminato, T., Urabe, T., Maeda, Y., 2011. Relation between single very-long-period pulses and volcanic gas emissions at Mt. Asama, Japan. Geophys. Res. Lett. 38, L11307, http://dx.doi.org/10.1029/2011GL047555.
Klug, C., Cashman, K.V., 1994. Vesiculation of May 18, 1980, Mount St. Helens magma. Geology 22, 468–472.
Klug, C., Cashman, K.V., 1996. Permeability development in vesiculating magmas: implications for fragmentation. Bull. Volcanol. 58, 87–100.

Kobayashi, T., Namiki, A., Sumita, I., 2010. Excitation of airwaves caused by bubble bursting in a cylindrical conduit: experiments and a model. J. Geophys. Res. 115, B10201, http://dx.doi.org/10.1029/2009JB006828.
Kozono, T., Koyaguchi, T., 2009. Effects of relative motion between gas and liquid on 1-dimensional steady flow in silicic volcanic conduits: 2. Origin of diversity of eruption styles. J. Volcano. Geotherm. Res. 180, 37–49.
Llewellin, E.W., Mader, H.M., Wilson, S.D.R., 2002. The rheology of a bubbly liquid. Proc. R. Soc. Lond. A 458, 987–1016.
Manga, M., Castro, J., Cashman, K.V., Loewenberg, M., 1998. Rheology of bubble-bearing magmas. J. Volcanol. Geotherm. Res. 87, 15–28.
Mangan, M., Sisson, T., 2005. Evolution of melt-vapor surface tension in silicic volcanic systems: experiments with hydrous melts. J. Geophys. Res. 110, B01202, http://dx.doi.org/10.1029/2004JB003215.
Melnik, O., Barmin, A.A., Sparks, R.S.J., 2005. Dynamics of magma flow inside volcanic conduits with bubble overpressure buildup and gas loss through permeable magma. J. Volcano. Geotherm. Res. 143, 53–68.
Mourtada-Bonnefoi, C.C., Laporte, D., 2004. Kinetics of bubble nucleation in a rhyolitic melt: an experimental study of the effect of ascent rate. Earth Planet. Sci. Lett. 218, 521–537.
Namiki, A., Manga, M., 2005. Response of a bubble bearing viscoelastic fluid to rapid decompression: implications for explosive volcanic eruptions. Earth Planet. Sci. Lett. 236, 269–284.
Namiki, A., Manga, M., 2008. Transition between fragmentation and permeable outgassing of low viscosity magmas. J. Volcanol. Geotherm. Res. 169, 48–60.
Noguchi, S., Toramaru, A., Nakada, S., 2008. Relation between microlite textures and discharge rate during the 1991–1995 eruptions at Unzen, Japan. J. Volcanol. Geotherm. Res. 175, 141–155.
Okumura, S., Nakamura, M., Nakano, T., Uesugi, K., Tsuchiyama, A., 2010. Shear deformation experiments on vesicular rhyolite: implications for brittle fracturing, degassing, and compaction of magmas in volcanic conduits. J. Geophys. Res. 115, B06201, http://dx.doi.org/10.1029/2009JB006904.
Okumura, S., Nakamura, M., Takeuchi, S., Tsuchiyama, A., Nakano, T., Uesugi, K., 2009. Magma deformation may induce non-explosive volcanism via degassing through bubble networks. Earth Planet. Sci. Lett. 281, 267–274.
Okumura, S., Nakamura, M., Tsuchiyama, A., Nakano, T., Uesugi, K., 2008. Evolution of bubble microstructure in sheared rhyolite: formation of a channel-like bubble network. J. Geophys. Res. 113, B07208, http://dx.doi.org/10.1029/2007JB005362.
Pal, R., 2003. Rheological behavior of bubble-bearing magmas. Earth Planet. Sci. Lett. 207, 165–179.
Parfitt, E.A., Wilson, L., 2008. Fundamentals of Physical Volcanology. Blackwell Publishing.
Princen, H.M., Kiss, A.D., 1989. Rheology of foams and highly concentrated emulsions: IV. An experimental study of the shear viscosity and yield stress of concentrated emulsions. J. Colloid Interface Sci. 128, 176–187.
Ripepe, M., Marchetti, E., Ulivieri, G., Harris, A., Dehn, J., Burton, M., Caltabiano, T., Salerno, G., 2005. Effusive to explosive transition during the 2003 eruption of Stromboli volcano. Geology 33, 341–344.
Rust, A.C., Manga, M., 2002a. Bubble shapes and orientations in low Re simple shear flow. J. Colloid Interface Sci. 249, 476–480.
Rust, A.C., Manga, M., 2002b. Effects of bubble deformation on the viscosity of dilute suspensions. J. Non-Newtonian Fluid Mech. 104, 53–63.
Schall, P., van Hecke, M., 2010. Shear bands in matter with granularity. Annu. Rev. Fluid Mech. 42, 67–88.
Shinohara, H., 2008. Excess degassing from volcanoes and its role on eruptive and intrusive activity. Rev. Geophys. 46, RG4005, http://dx.doi.org/10.1029/2007RG000244.
Stone, H.A., 1994. Dynamics of drop deformation and breakup in viscous fluids. Annu. Rev. Fluid Mech. 26, 65–102.
Takeuchi, S., 2011. Pre-eruptive magma viscosity: an important measure of magma eruptibility. J. Geophys. Res. 116, B10201, http://dx.doi.org/10.1029/2011JB008243.
Takeuchi, S., Tomiya, A., Shinohara, H., 2009. Degassing conditions for permeable silicic magmas: implications from decompression experiments with constant rates. Earth Planet. Sci. Lett. 283, 101–110.
Taylor, G.I., 1934. The formation of emulsions in definable fields of flow. Proc. R. Soc. Lond. A 146, 501–523.
Tuffen, H., Smith, R., Sammonds, P.R., 2008. Evidence for seismogenic fracture of silicic magma. Nature 453, 511–514.
Voight, B., Sparks, R.S.J., Miller, A.D., Stewart, R.C., Hoblitt, R.P., Clarke, A., Ewart, J., Aspinall, W.P., Baptie, B., Calder, E.S., Cole, P., Druitt, T.H., Hartford, C., Herd, R.A., Jackson, P., Lejeune, A.M., Lockhart, A.B., Loughlin, S.C., Luckett, R., Lynch, L., Norton, G.E., Robertson, R., Watson, I.M., Watts, R., Young, S.R., 1999. Magma flow instability and cyclic activity at Soufriere Hills Volcano, Montserrat, British West Indies. Science 283, 1138–1142.
Wallace, P.J., 2001. Volcanic SO_2 emissions and the abundance and distribution of exsolved gas in magma bodies. J. Volcanol. Geotherm. Res. 108, 85–106.
Wang, Y., Krishan, K., Dennin, M., 2006. Impact of boundaries on velocity profiles in bubble rafts. Phys. Rev. E 73, 031401.
Webb, S.L., Dingwell, D.B., 1990. Non-newtonian rheology of igneous melts at high stresses and strain rates: experimental results for rhyolite, andesite, basalt, and nephelinite. J. Geophys. Res. 95, 15695–15701.